MIXED CONVECTION BOUNDARY LAYER FLOW OF A VISCOELASTIC FLUID DUE TO HORIZONTAL ELLIPTIC CYLINDER WITH CONSTANT HEAT FLUX

Tariq JAVED [a1], ***Hussain AHMAD*** [a], ***and Abuzar GHAFFARI*** [b]

[a] Department of Mathematics and Statistics, FBAS, International Islamic University, Islamabad 44000, Pakistan

[b] Department of Mathematics, University of Education, Attock Campus 43600, Pakistan

Abstract: *This article presents numerical analysis of mixed convection laminar flow of a second grade viscoelastic fluid due to cylinder of elliptic cross-section with prescribed surface heat flux. Dimensionless nonlinear analysis is computed employing Keller-box method. Skin friction coefficient and Nusselt number are emphasized specifically. These quantities are displayed graphically to examine their behavior along the surface of cylinder. The flow and heat transfer rates are carefully judged while varying the important resulting parameters (Mixed convection parameter, viscoelastic parameter aspect ratio etc.) through sketched graphs keeping major axis of ellipse along and perpendicular to the horizontal. These two positions of major axis are termed as blunt and slender orientations respectively. The values of skin friction and Nusselt number increase with rise in mixed convection parameter. On the other hand, these quantities lessen by increasing the value of viscoelastic parameter.*

Keywords*: Mixed convection, viscoelastic boundary layer flow, elliptic cylinder, aspect ratio, Numerical solution.*

1. Introduction

Convective flows with heat transfer are of much interest to the recent researchers from both theoretical and practical point of view. Such interest stems due to the occurrence of these flows in geophysical and engineering fields including solid matrix heat exchangers, ground water movement, geothermal energy extraction, oil and gas production, thermal insulation drying porous solids, nuclear waste disposals and many others. Especially mixed convection flows are important in numerous physical situations in environment as well as in artificial appliances e.g. cooling of semi-conductor devices and nuclear power houses etc. For the efficient working of the electronic devices, the cooling through air streams is very easy and economical. To retain working temperature of a system in the industries natural convection and external currents of air are effectively used. The combination of an external source of pushing air and natural convection termed as mixed convection flow. Therefore, the importance of study of mixed convection is recognizable due to its occurrence in nature and in many engineering applications. One of the most important applications of mixed convection flows is cooling of heat exchangers' components. Elliptic cylinder shapes are commonly used in the heat exchangers. These cylindrical shapes with elliptic cross-section offer smaller resistance to air to pass through and effectively cool the system. Thus, the discovery of efficient and reliable heat exchangers requires a detailed investigation and a careful consideration of heat flows over this kind of geometry. An encyclopedic literature dealing with mixed convection laminar flows over circular cylinder is available but scrutiny of mixed convection flows over the elliptic cylinder needs some serious attention. The pioneering work regarding free convection flows over

[1] E-mail address: tariq_17pk@yahoo.com

elliptic cylinder with PST and PHF was carried out by Merkin [1]. He investigated heat flow over elliptic cylinder of different eccentricities for both blunt orientation (major axis along horizontal) and slender orientation (major axis along vertical). In another paper, Merkin [2] investigated mixed convection flows over horizontal circular cylinder with PST condition. Bhatacharyya and Pop [3] discussed free convection heat transfer from an elliptical cylinder in flow of micropolar fluids. Hossain et al [4] invented radiation effect over steady natural convection flow over elliptic geometry. Ahmad et al. [5] reproduced results of Merkin [1] for constant heat flux case successfully using Keller-box scheme. They presented theoretical results for both air and water to get the concordance with experimental results. Javed et al. [6] presented effect of thermal radiation on unsteady mixed convection flow near forward stagnation point over cylinder of elliptic cross-section. They numerically simulated the problem using Keller-box method and calculated the solution at different time steps. Recently, Javed et al. [7] discovered mixed convection flow around the elliptic cylinder. In this article, they presented the solution by considering stream velocity as a sine function of eccentric angle. Moreover, a useful contribution in this regards can be seen in the references [8-11].

The study of viscoelastic fluid flows has also a great importance due to its applications in engineering and several manufacturing processes e.g. petroleum drilling, manufacturing of food, paper, paints, coating, inks and jet fuels etc. The viscoelastic fluid is of second grade nature. Dun and Rajagopal [12] did a comprehensive discussion on second and third order fluids. Ariel [13] and Rajagopal et al [14] also studied viscoelastic fluids in different geometries. It is also necessary here to mention the work done by Cortell [15], Abel et al [16], Hayat et al. [17] and Sajid et al. [18] on second grade fluids. Recently, Abbas et al. [19-21] discussed the hydromagnetic flow of viscoelastic fluid in stretching/shrinking sheet and in semi-porous channel separately. Anwar et al. [22] studied the steady mixed convection boundary layer flow of viscoelastic fluid over a horizontal circular cylinder with constant surface temperature. Later on, Kasim et al. [23] investigated the constant heat solution for the viscoelastic boundary layer flow on circular cylinder. Ahmad et al. [24] reported on radiation effect on boundary layer flow of a viscoelastic fluid over the circular cylinder.

After the persuasion of above referred work we extended the idea presented in [7] for the second grade viscoelastic fluid model over surface of the cylinder of elliptic cross-section with PHF condition. The drawn numerical outcomes are matched with those presented by Kasim et al. [23] for the validation of our solution procedure. This study demonstrated the consequences resulted by varying the emerging parameters on flow and heat transfer rates for both orientations.

2. Mathematical analysis

Let us take an elliptic cylinder lying horizontally and consider laminar mixed convection flow of an incompressible, second grade viscoelastic fluid over it. In addition, let lengths of major and minor axis are 2*a* and 2*b* respectively. Suppose the fluid be moving with a constant free stream velocity $U_\infty / 2$ in the upward direction in such a way that velocity at the edge of boundary layer is $\bar{u}_e$. T_∞ stands for temperature of ambient fluid and let the surface of cylinder be emitting a constant heat flux q_w. The schematic diagram of the problem is given in Fig.1. The conditions on surface heat flux are $q_w > 0$ and $q_w < 0$ which represent the assisting and opposing flow cases respectively. The horizontal cylinder is considered enough long to discard end effects. This assumption gives flow field to be two-dimensional. Along with these assumptions and Boussinesq and boundary layer approximations, the basic equations [22-24] are

$$\frac{\partial \bar{u}}{\partial \bar{x}} + \frac{\partial \bar{v}}{\partial \bar{y}} = 0, \tag{1}$$

$$\bar{u}\frac{\partial \bar{u}}{\partial \bar{x}}+\bar{v}\frac{\partial \bar{u}}{\partial \bar{y}}=\bar{u}_e\frac{\partial \bar{u}_e}{\partial \bar{x}}+\nu\frac{\partial^2 \bar{u}}{\partial \bar{y}^2}+\frac{k_0}{\rho}\left(\frac{\partial \bar{u}}{\partial \bar{x}}\frac{\partial^2 \bar{u}}{\partial \bar{y}^2}+\bar{u}\frac{\partial^3 \bar{u}}{\partial \bar{x}\partial \bar{y}^2}+\bar{v}\frac{\partial^3 \bar{u}}{\partial \bar{y}^3}-\frac{\partial \bar{u}}{\partial \bar{y}}\frac{\partial^2 \bar{u}}{\partial \bar{x}\partial \bar{y}}\right)+g\beta(\bar{T}-T_\infty)\sin\phi, \quad (2)$$

$$\rho C_p\left(\bar{u}\frac{\partial \bar{T}}{\partial \bar{x}}+\bar{v}\frac{\partial \bar{T}}{\partial \bar{y}}\right)=k\frac{\partial^2 \bar{u}}{\partial \bar{y}^2} \quad (3)$$

where the symbols used are given in the list blow:

$\bar{x}$, $\bar{y}$: Cartesian coordinates

$\bar{u}$, $\bar{v}$: velocity components along $\bar{x}$ and $\bar{y}$

$\bar{T}$: temperature

ν :kinematic viscosity

ρ :density

C_p : specific heat constant

k : thermal conductivity of the fluid

k_0 : viscoelastic material parameter

g : gravitational acceleration

β : thermal expansion coefficient

ϕ : angle measured between downward vertical and outer perpendicular

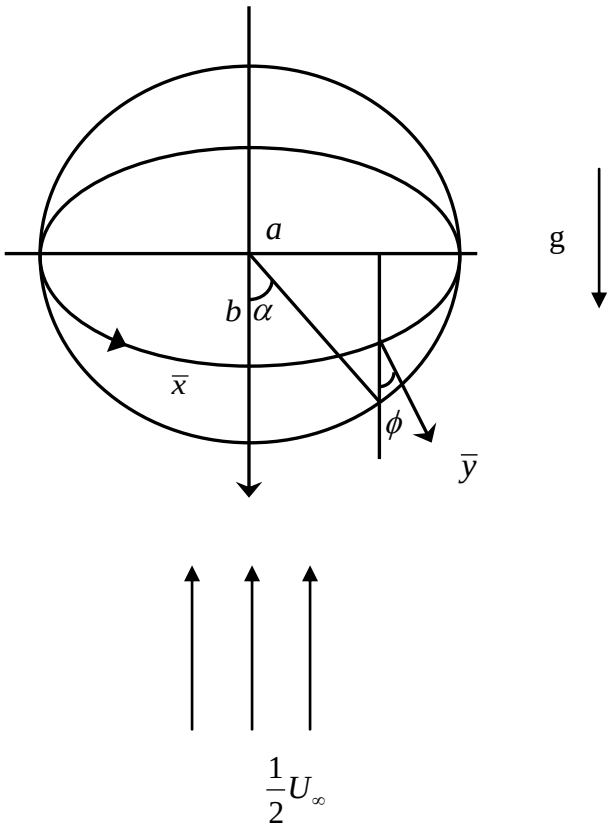

Fig. 1: Schematic diagram of problem

In the present study, k_0 is taken positive to meet thermodynamic conditions as it was suggested by Dunn and Rajagopal [12]. The Newtonian case can be restored by setting $k_0 = 0$. The related boundary conditions are given by

$$\bar{u}=0,\ \bar{v}=0,\ \frac{\partial \bar{T}}{\partial \bar{y}}=-\frac{q_w}{k} \qquad at\ \bar{y}=0,$$
$$\bar{u}\to\bar{u}_e,\bar{T}\to T_\infty \qquad as\ \bar{y}\to\infty. \quad (4)$$

The boundary condition on $\bar{u}$ are two in number but the governing equations representing the problem involve

third order derivative of $\bar{u}$ which demands one extra boundary condition. Garg and Rajagopal [25] that extra boundary condition i.e. $\partial\bar{u}/\partial\bar{y} \to 0$ when $\bar{y} \to \infty$, which suffices for the solution of boundary value problem comprising eqs. (1-4).

Now introducing the following non-dimensional variables.

$$x = \frac{\bar{x}}{a},\ y = \mathrm{Re}^{\frac{1}{2}}\left(\frac{\bar{y}}{a}\right),\ u = \frac{\bar{u}}{U_\infty},\ v = \mathrm{Re}^{\frac{1}{2}}\left(\frac{\bar{v}}{U_\infty}\right),\ \theta = \frac{\mathrm{Re}^{\frac{1}{2}}k}{aq_w}(\bar{T} - T_\infty),\ u_e = \frac{\bar{u}_e}{U_\infty}, \tag{5}$$

into Eqs. (1-3) we arrive at

$$\frac{\partial u}{\partial x} + \frac{\partial v}{\partial y} = 0, \tag{6}$$

$$u\frac{\partial u}{\partial x} + v\frac{\partial v}{\partial y} = u_e\frac{du_e}{dx} + \frac{\partial^2 u}{\partial y^2} + K\left(\frac{\partial u}{\partial x}\frac{\partial^2 u}{\partial y^2} + u\frac{\partial^3 u}{\partial x\partial y^2} + v\frac{\partial^3 u}{\partial y^3} - \frac{\partial u}{\partial y}\frac{\partial^2 u}{\partial x\partial y}\right) + \lambda\sin\phi\theta, \tag{7}$$

$$u\frac{\partial\theta}{\partial x} + v\frac{\partial\theta}{\partial y} = \frac{1}{\mathrm{Pr}}\frac{\partial^2\theta}{\partial y^2}. \tag{8}$$

where $\mathrm{Re} = aU_\infty/\nu$ (Reynolds number), $K = \frac{k_0 U_\infty}{a\rho\nu}$ (viscoelastic parameter), $\lambda = Gr\Big/\mathrm{Re}^{\frac{5}{2}}$ (mixed convection parameter) and $\mathrm{Pr} = \frac{\mu C_p}{k}$ (Prandtl number) respectively with $Gr = \frac{g\beta q_w a^4}{k\nu^2}$ (Grashof number).

The mixed convection parameter λ in form of Gr gives that with $\lambda > 0$ and $\lambda < 0$ define assisting flow case and opposing flow case correspondingly. The case $K = 0$ restores the Newtonian flow problem.

The boundary conditions (4) along the augmented boundary condition reduces to following form

$$\begin{gathered} u = v = 0,\ \frac{\partial\theta}{\partial y} = -1 \text{ at } y = 0, \\ u \to u_e,\ \frac{\partial u}{\partial y} \to 0,\ \theta \to 0 \text{ as } y \to \infty. \end{gathered} \tag{9}$$

Next we assume the free stream velocity $u_e(\alpha) = \sin\alpha$ where α is the eccentric angle of the ellipse (see Fig.1) and introducing the following variables to solve the problem.

$$\psi = xf(x,y),\ \theta = \theta(x,y), \tag{10}$$

with ψ being the usual stream defined by

$$u = \frac{\partial\psi}{\partial y},\ v = -\frac{\partial\psi}{\partial x}, \tag{11}$$

With these assumptions eq.(6) is identically satisfied and the boundary value problem represented by eqs. (7-9) reduces to the following forms:

$$\begin{aligned} &\frac{\partial^3 f}{\partial y^3} + f\frac{\partial^2 f}{\partial y^2} - \left(\frac{\partial f}{\partial y}\right)^2 + \frac{\sin\alpha\cos\alpha}{xB} + \lambda\frac{\sin\phi}{x}\theta - K\left[f\frac{\partial^4 f}{\partial y^4} - 2\frac{\partial f}{\partial y}\frac{\partial^3 f}{\partial y^3} + \left(\frac{\partial^2 f}{\partial y^2}\right)^2\right. \\ &\left. + x\left(\frac{\partial f}{\partial x}\frac{\partial^4 f}{\partial y^4} - \frac{\partial^2 f}{\partial x\partial y}\frac{\partial^3 f}{\partial y^3} + \frac{\partial^2 f}{\partial y^2}\frac{\partial^3 f}{\partial x\partial y^2} - \frac{\partial f}{\partial y}\frac{\partial^4 f}{\partial x\partial y^3}\right)\right] = x\left(\frac{\partial f}{\partial y}\frac{\partial^2 f}{\partial x\partial y} - \frac{\partial f}{\partial x}\frac{\partial^2 f}{\partial y^2}\right), \end{aligned} \tag{12}$$

$$\frac{1}{\mathrm{Pr}}\frac{\partial^2\theta}{\partial y^2} + f\frac{\partial\theta}{\partial y} = x\left(\frac{\partial f}{\partial y}\frac{\partial\theta}{\partial x} - \frac{\partial f}{\partial x}\frac{\partial\theta}{\partial y}\right), \tag{13}$$

$$f = \frac{\partial f}{\partial y} = 0,\ \frac{\partial \theta}{\partial y} = -1 \text{ at } y = 0,$$
$$\frac{\partial f}{\partial y} \to \frac{\sin\alpha}{x},\ \frac{\partial^2 f}{\partial y^2} \to 0,\ \theta \to 0 \text{ as } y \to \infty. \tag{14}$$

The geometry shown in fig.1 clearly demonstrates that when $\sin\phi = \sin x$ .the elliptic cylinder reduces to circular cylinder. The study of elliptic cylinder case is confined to two possible cases namely the blunt orientation and slender orientation when major axis of ellipse is considered along horizontal and perpendicular to it respectively [1]. The quantities given in eq. (12) x, $\sin\phi$ and B are parametrically for blunt as well as slender orientations are

$$x = \int_0^{\alpha} (1 - e^2 \sin^2\lambda)^{\frac{1}{2}} d\lambda,\ \sin\phi = \frac{b\sin\alpha}{a(1 - e^2\sin^2\alpha)^{\frac{1}{2}}} \text{ and } B = (1 - e^2\sin^2\alpha)^{\frac{1}{2}}$$

and

$$x = \int_0^{\alpha} (1 - e^2 \cos^2\lambda)^{\frac{1}{2}} d\lambda,\ \sin\phi = \frac{\sin\alpha}{(1 - e^2 cos^2\alpha)^{\frac{1}{2}}} \text{ and } B = (1 - e^2 cos^2\alpha)^{\frac{1}{2}}$$

respectively.

With $e^2 = 1 - \frac{b^2}{a^2}$ which is square of the eccentricity *e* of the ellipse.

The demanding physical quantities skin-friction coefficient C_f and the Nusselt number Nu are defined by

$$C_f = \frac{\tau_w}{\rho U_\infty^{\ 2}},\ Nu = \frac{a q_w}{k(\overline{T} - T_\infty)} \tag{15}$$

where τ_w and q_w express the wall shear stress and surface heat flux respectively which satisfy

$$\tau_w = \mu\left(\frac{\partial \overline{u}}{\partial \overline{y}}\right)_{\overline{y}=0} + k_0\left(\overline{u}\frac{\partial^2 \overline{u}}{\partial \overline{x}\partial \overline{y}} + \overline{v}\frac{\partial^2 \overline{u}}{\partial \overline{y}^2} + 2\frac{\partial \overline{u}}{\partial \overline{x}}\frac{\partial \overline{u}}{\partial \overline{y}}\right)_{\overline{y}=0},\ q_w = -k\left(\frac{\partial \overline{T}}{\partial \overline{y}}\right)_{\overline{y}=0}. \tag{16}$$

Using Eqs. (4) and (10), we get

$$C_f\,\mathrm{Re}^{\frac{1}{2}} = x\left(\frac{\partial^2 f}{\partial y^2}\right)_{y=0},\ Nu\,\mathrm{Re}^{-\frac{1}{2}} = \frac{1}{\theta(x,0)}. \tag{17}$$

The limiting case i.e. at the lower stagnation point of the cylinder $x \approx 0$, the partial differential equations (12) and (13) along the boundary conditions to the ordinary differential equations

$$f''' + ff'' - (f')^2 + L + \lambda A_0\theta - K\left[ff^{iv} - 2f'f''' + (f'')^2\right] = 0, \tag{18}$$

$$\frac{1}{\mathrm{Pr}}\theta'' + f\theta' = 0, \tag{19}$$

With boundary condition

$$f(0) = f'(0) = 0,\ \theta'(0) = -1 \text{ and}$$
$$f' \to 1,\ f'' \to 0,\ \theta \to 0 \text{ as } y \to \infty, \tag{20}$$

the prime notation gives rate of change with respect to y and the quantities $\frac{\sin\alpha\cos\alpha}{x.B}$, $\frac{\sin\phi}{x}$ approach to *L* and A_0 respectively as $x \to 0$ These quantities take the following values $L = 1$, $A_0 = \frac{b}{a}$ for the blunt orientation and $L = A_0 = \frac{a^2}{b^2}$ for the slender orientation.

The eq.(17) reduces to following form

$$C_f \,\mathrm{Re}^{\frac{1}{2}} = xf''(0),\ Nu\,\mathrm{Re}^{-\frac{1}{2}} = \frac{1}{\theta(0)}. \tag{21}$$

3. Numerical solution

This section demonstrates the numerical discretization and numerical procedure adopted for the solution of the problem. An implicit finite difference scheme given by Keller and Cebeci [26] is implemented for the solution of governing P.D.E.'s (12-13) with B.C.'s (14). This numerical procedure is very well explained in the book of Cebeci and Bradshaw [27].The equations are discretized along the whole domain by selecting a suitably small step size in both *x* and *y* directions. The grid size Δy = 0.02 and $\Delta x = \pi/180$ is found suitable for the present study. The accuracy of achieved results are validated through the benchmark [28] and [23] by setting Pr = 1, *b/a* =1 (circular cylinder case) and *K* = 0 (Newtonian case). Table 1 shows an excellent concordance of our computed results with the results above referred. In this procedure all higher order P.D.E's are reduced to the first order P.D.E's. So, the following variables are introduced

$$f_y = u,\ f_{yy} = v,\ f_{yyy} = w,\ f_{yyyy} = g, \text{and}\ \theta_y = q$$

then the governing eqs. (12-14) reduces to

$$v' + fv - u^2 + \frac{\sin\alpha\cos\alpha}{x.B} + \lambda\frac{\sin\phi}{x}\theta - K\left[fg - 2uw + v^2 + x\left(ug - w\frac{\partial u}{\partial x} + v\frac{\partial v}{\partial x} - u\frac{\partial w}{\partial x}\right)\right] - x\left(u\frac{\partial u}{\partial x} - v\frac{\partial f}{\partial x}\right) = 0$$

$$\frac{1}{\mathrm{Pr}}q' + fq - x\left(u\frac{\partial\theta}{\partial x} - q\frac{\partial f}{\partial x}\right) = 0$$

$$f(x,0) = u(x,0) = 0, q(x,0) = -1$$

$$u(x,\infty) = \frac{\sin\alpha}{x}, v(x,\infty) = 0, \theta(x,\infty) = 0$$

The uniform grid points are taken in (x,y) plane which are defined as

$$x^0 = 0, x^n = x^{n-1} + k, y_0 = 0, y_j = y_{j-1} + h$$

where

$$j = 1, 2, \ldots\ldots M \text{ and } n = 1, 2, \ldots\ldots\ldots N$$

with *n* and *j* being positive integers showing the grid location in the (*x*,*y*). The derivatives with respect to *x* and *y* are discretized by the formulas given below

$$(\,)_j^{n-\frac{1}{2}} = \frac{1}{k}\left((\,)_j^n - (\,)_j^{n-1}\right) \text{ and } (\,)_{j-\frac{1}{2}}^n = \frac{1}{h}\left((\,)_j^n - (\,)_{j-1}^n\right)$$

and the function's value is taken as average value at two consecutive grid points

$$(\,)_j^{n-\frac{1}{2}} = \frac{1}{2}\left((\,)_j^n + (\,)_j^{n-1}\right) \text{ and } (\,)_{j-\frac{1}{2}}^n = \frac{1}{2}\left((\,)_j^n + (\,)_{j-1}^n\right)$$

The Newton's linearization is employed to linearize highly nonlinear P.D.E's in the following fashion

$$\left(f_j^n\right)^{i+1} = \left(f_j^n\right)^i + \left(\delta f_j^n\right)^i, \left(u_j^n\right)^{i+1} = \left(u_j^n\right)^i + \left(\delta u_j^n\right)^i,$$

$$\left(v_j^n\right)^{i+1} = \left(v_j^n\right)^i + \left(\delta v_j^n\right)^i, \left(w_j^n\right)^{i+1} = \left(w_j^n\right)^i + \left(\delta w_j^n\right)^i,$$

$$\left(g_j^n\right)^{i+1} = \left(g_j^n\right)^i + \left(\delta g_j^n\right)^i, \left(\theta_j^n\right)^{i+1} = \left(\theta_j^n\right)^i + \left(\delta\theta_j^n\right)^i \text{ and}$$

$$\left(q_j^n\right)^{i+1} = \left(q_j^n\right)^i + \left(\delta q_j^n\right)^i$$

By supplying a suitable initial guess, we obtain a linear system of algebraic equations, which is solved using tri-diagonal elimination to get the solution at next grid point.

4. Results and discussion

The non-dimensional P.D.E.'s (12-13) with B.C.'s (14) and O.D.E's (18-19) with B.C's (20) are integrated numerically using an implicit finite difference scheme i.e. Keller-box method. The details of the scheme are given in the references [26] and [27]. The grid size along y direction Δy and y_∞ is carefully varied adjusted for various choices of pertinent parameters to get highly accurate results. Therefore, the grid size $\Delta y = 0.02$ and $\Delta x = \pi/180$ has found suitable for present numerical study. The calculations of results are started at lower stagnation point and continue the process along the surface of cylinder to the point where solution exists and separation does not occur. To assure the accuracy of computed results, we have matched them to those earlier reported by Kasim et al. [23] and Nazar et al [28] setting $\Pr = 1$, $b/a = 1$ (circular cylinder case) and $K = 0$ (Newtonian case). Table 1 shows an excellent concordance of our computed results with above referred results.

λ		$f''(0)$			$\theta(0)$	
	[28]	[23]	Present	[28]	[23]	Present
-0.7	-	0.247743	0.24794	-	2.220434	2.2201
-0.6	0.4925	0.490622	0.49056	2.0547	2.057117	2.0572
-0.4	0.7998	0.798697	0.79866	1.9046	1.906045	1.9061
-0.2	1.0340	1.033028	1.033	1.8157	1.816890	1.8169
0	1.2336	1.232658	1.2326	1.7517	1.752872	1.7529
0.2	1.4117	1.410764	1.4107	1.7018	1.702823	1.7029
0.4	1.5747	1.573759	1.5737	1.6608	1.661736	1.6618
0.6	1.7263	1.725350	1.7253	1.6260	1.626904	1.6269
0.8	1.8690	1.867919	1.8679	1.5958	1.596697	1.5967
1.0	2.0042	2.003106	2.0031	1.5692	1.570047	1.5701
1.4	2.2570	1.255786	2.2557	1.5239	1.524693	1.5247
1.8	2.4913	2.489892	2.4898	1.4863	1.487048	1.4871
3.0	3.1171	3.115282	3.1152	1.4015	1.402232	1.4022
4.0	3.5784	3.576073	3.576	1.3500	1.350735	1.3507
5.0	4.0019	3.999106	3.999	1.3088	1.309546	1.3096
6.0	4.3967	4.393430	4.3933	1.2746	1.275348	1.2754
7.0	4.7686	4.764909	4.7647	1.2455	1.246194	1.2462
8.0	5.1217	5.117609	5.1174	1.2201	1.220844	1.2209
9.0	5.4591	5.454494	5.4543	1.1977	1.198462	1.1985
10.0	5.7730	5.777805	5.7776	1.1770	1.178456	1.1785

Table 1: The values of $f''(0)$ and $\theta(0)$ for various values of λ with $\Pr = 1$, $b/a = 1$ and $K = 0$ (Newtonian fluid)

The profiles of key physical quantities- the skin friction $C_f \operatorname{Re}^{\frac{1}{2}}$ and Nusselt number $Nu \operatorname{Re}^{-\frac{1}{2}}$ for blunt orientation case are displayed in figs. (2-5). Figs. 2 (*a*,*b*) illustrate the $C_f \operatorname{Re}^{\frac{1}{2}}$ and $Nu \operatorname{Re}^{-\frac{1}{2}}$ for various options while other parameters are kept fixed. It is noted that by the enhancement of the value of mixed convection parameter both flow and heat transfer rates boost. Also due to this increase in mixed convection, boundary layer separation delays. It is further seen that the flow rate achieves its maximum value along the surface of cylinder before separation initiates.

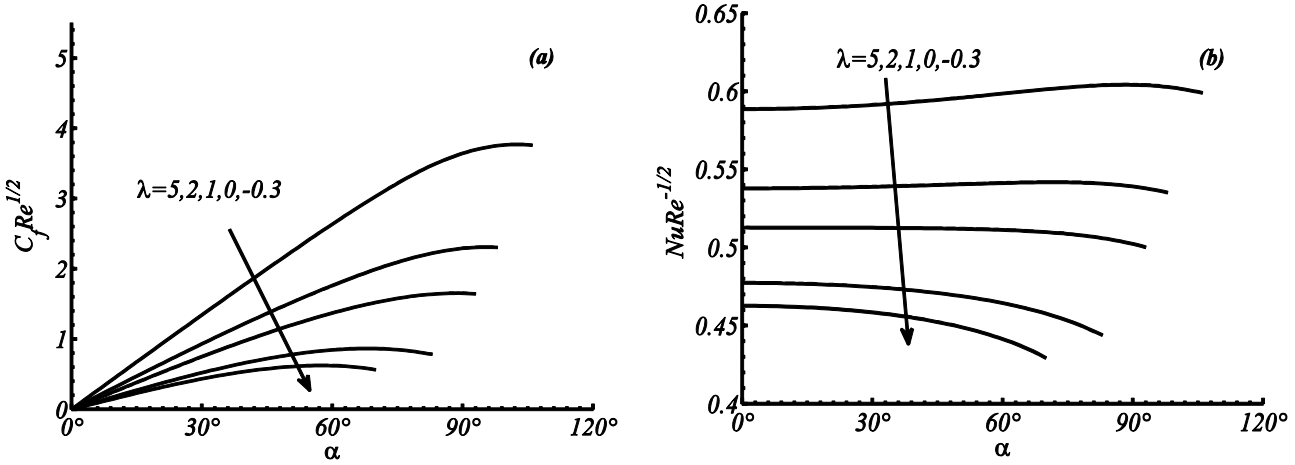

Figs. 2**(*a*,*b*):** The change in $C_f \,\mathrm{Re}^{\frac{1}{2}}$ and $Nu\,\mathrm{Re}^{-\frac{1}{2}}$ for various values mixed convection parameter λ when $K = 0.2$, $b/a = 0.5$ and $\mathrm{Pr} = 0.7$.

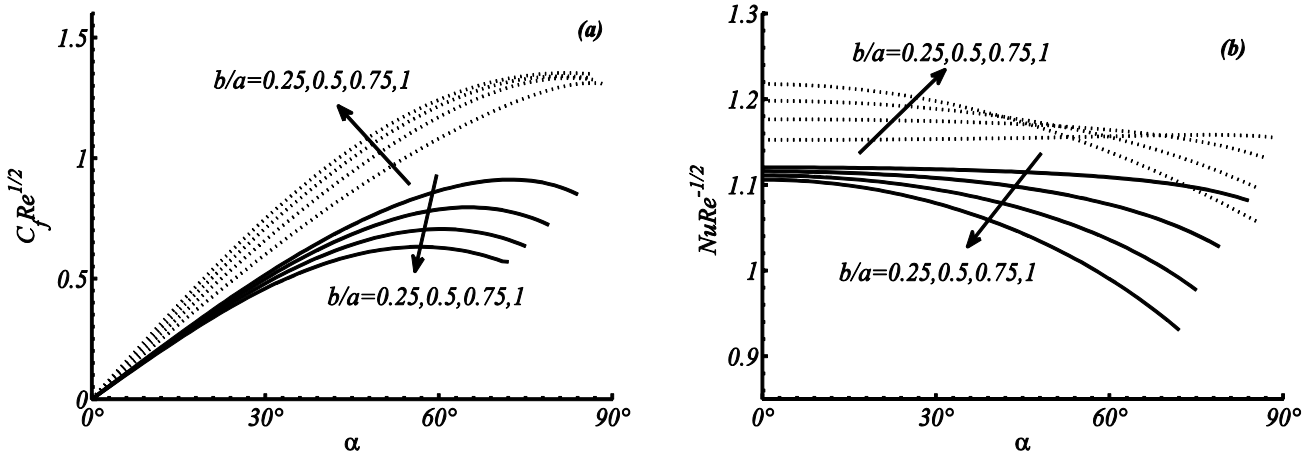

Figs. 3(*a*,*b*):. The change in $C_f \,\mathrm{Re}^{\frac{1}{2}}$ and $Nu\,\mathrm{Re}^{-\frac{1}{2}}$ for separate values of aspect ratio $\frac{b}{a}$ when $K = 0.2$, $\lambda = -0.3$ (solid curves), $\lambda = 2$ (dotted curves), and $\mathrm{Pr} = 7$.

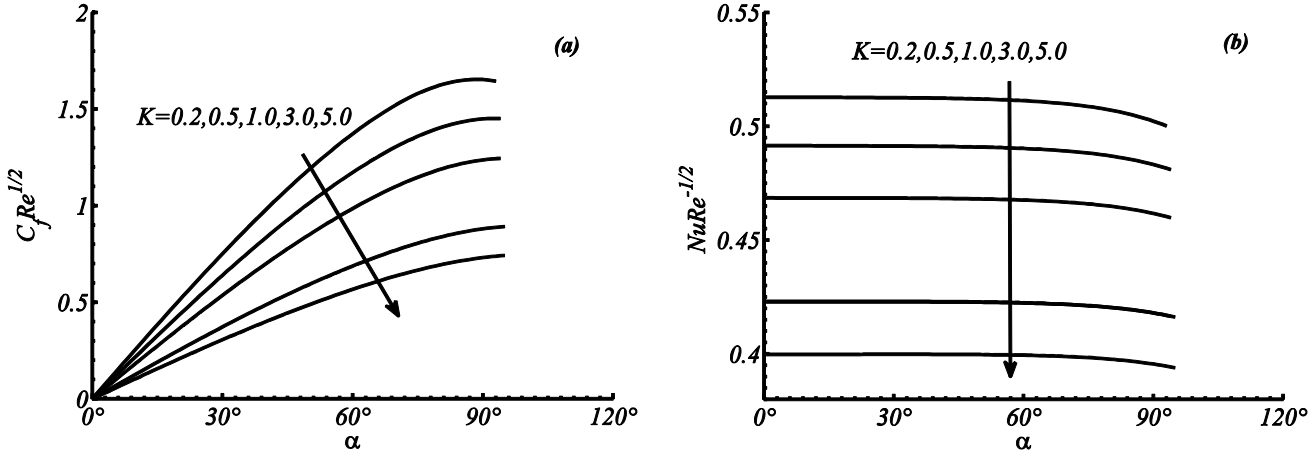

Figs. 4(*a*,*b*): The change in $C_f \,\mathrm{Re}^{\frac{1}{2}}$ and $Nu\,\mathrm{Re}^{-\frac{1}{2}}$ for various values of viscoelastic parameter K when $\lambda = 1$, $b/a = 0.5$ and $\mathrm{Pr} = 1$.

d

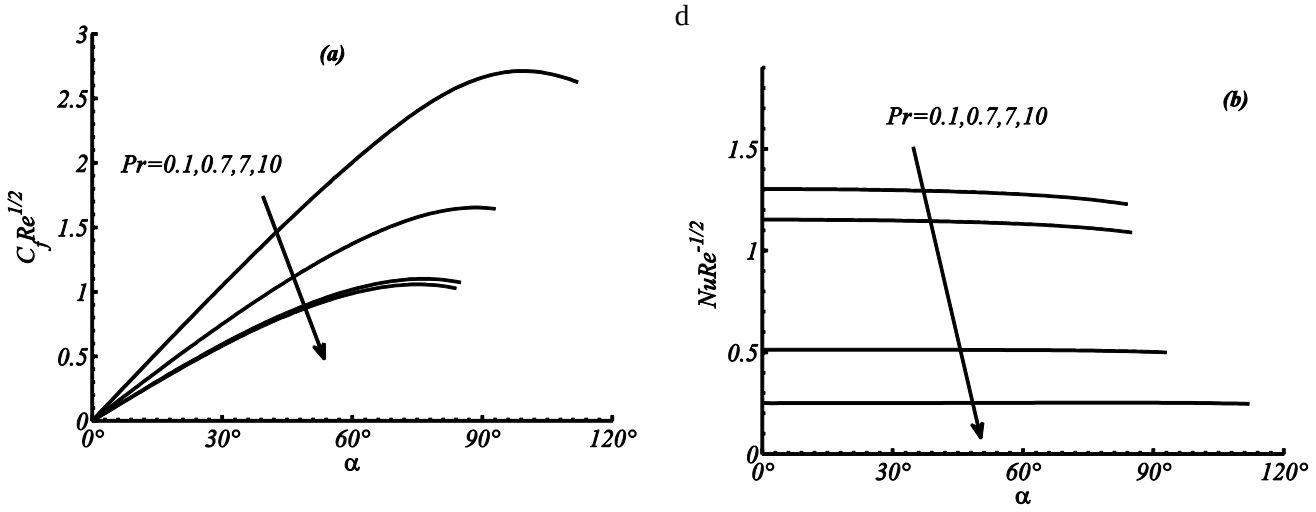

Figs. 5(*a,b*): The change in $C_f \,\mathrm{Re}^{\frac{1}{2}}$ and $Nu\,\mathrm{Re}^{-\frac{1}{2}}$ for various values of Prandtl number Pr when $\lambda = 1$, $b/a = 0.5$ and $K = 0.2$.

Figs. 3 (*a,b*) indicate the behavior of $C_f \,\mathrm{Re}^{\frac{1}{2}}$ and $Nu\,\mathrm{Re}^{-\frac{1}{2}}$ along the surface of cylinder for various choices of aspect ratio *b/a* both in the cooled cylinder case ($\lambda = -0.3$) and heated cylinder case ($\lambda = 2$). The solid curves give the trend of these quantities in cooled cylinder case and dotted curves express them in heated cylinder case. It is observed that by extending aspect ratio *b/a*, both flow and heat transfer rates decrease in the cooled cylinder case and boundary layer separation comes early. On the other hand, the same quantities show the reverse trend by extending the aspect ratio. A slight rise in the flow rate is noted by increasing the aspect ratio *b/a* . The heat transfer rate grows along the surface of cylinder in the interval $0 < \alpha < 42^\circ$ but declines in the interval $69^\circ < \alpha < 86^\circ$ by extending the aspect ratio of the elliptic cylinder. The change of behavior of heat transfer rate is shown in the interval $42^\circ < \alpha < 69^\circ$ by extending the aspect ratio. Figs. 4(*a,b*) express the trend of flow and heat transfer rates along the surface of cylinder for various options of viscoelastic parameter K while keeping the other parameters fixed. Both flow and heat transfer rates obviously decrease by the growth of viscoelastic parameter that agrees with the practical situations. Figs. 5(*a,b*) show the impact of Prandtl number Pr on flow and heat transfer rates along the surface of cylinder. Both quantities decrease due to rise in the value of Pr, but the boundary layer separation delays by lessening the value of Pr.

The flow and heat transfer rates in case of slender orientation are displayed in Figs. (6-10). The rise in flow and heat transfer rates due to growth of mixed convection parameter λ along the surface of cylinder. The phenomenon is displayed in figs.6 (*a,b*). It is interestingly noted that by raising the mixed convection parameter λ to a specific value λ_c the boundary layer separation delays. But the separation initiates early for $\lambda > \lambda_c$. The increase in flow and heat transfer rates due to the extension of aspect ratio for the range $0<b/a<0.5$ but decrease in the value of both quantities for *b/a* in the range $0.5<b/a<1$ is noticed in the cooled cylinder case. This fact is shown in Figs.7 (*a,b*). Figs. 8(*a,b*) illustrate the trend of flow and heat transfer rates for the different choices of the aspect ratio in case of heated cylinder. It is noticed that the flow rate increases but heat transfer rate decreases by extending the aspect ratio. The boundary layer separation delays on the other hand. Figs. 9 (*a,b*) indicate the effect of viscoelastic parameter on flow and heat transfer rates. Obviously, both quantities decrease due to the growth in value of viscoelasticity of the fluid as in case of blunt orientation.

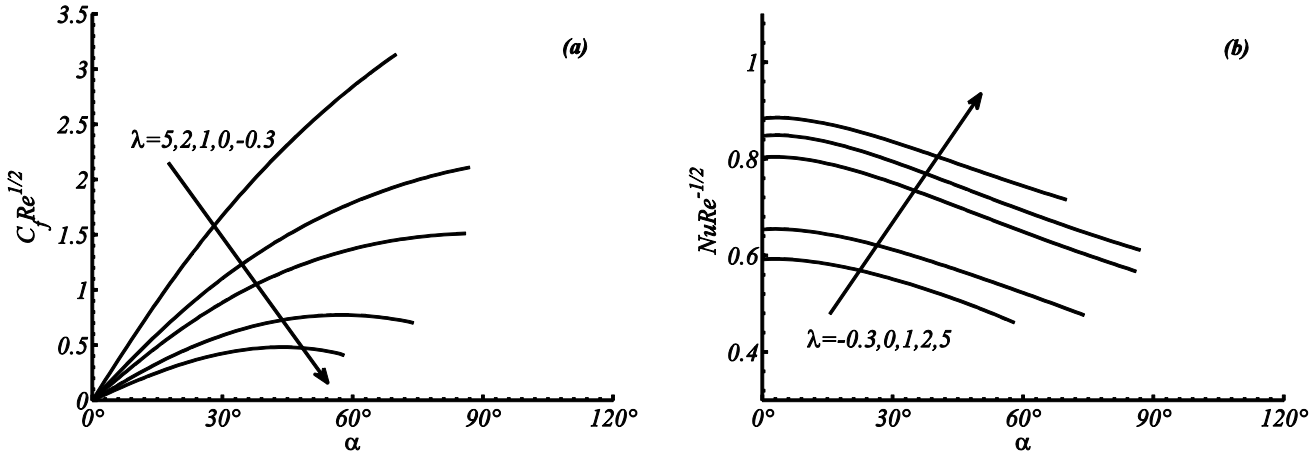

Figs. 7(*a*,*b*): The variation of $C_f \,\mathrm{Re}^{\frac{1}{2}}$ and $Nu\,\mathrm{Re}^{-\frac{1}{2}}$ for different values of mixed convection parameter λ when $K = 0.2$, $b/a = 0.5$ and $\mathrm{Pr} = 0.7$.

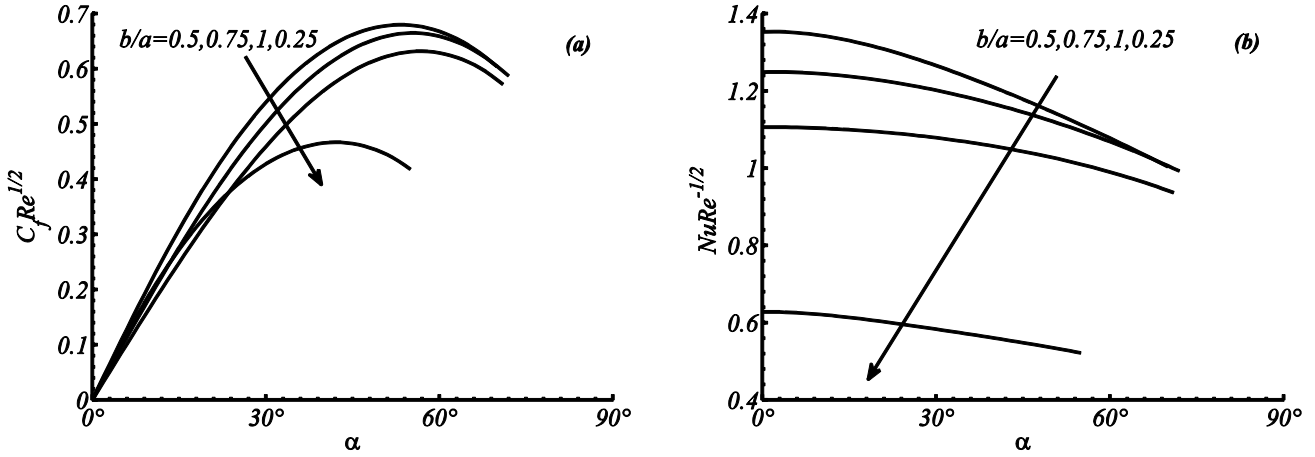

Figs. 8(*a*,*b*): The variation of $C_f \,\mathrm{Re}^{\frac{1}{2}}$ and $Nu\,\mathrm{Re}^{-\frac{1}{2}}$ for different values of aspect ratio $\frac{b}{a}$ when $K = 0.2$, $\lambda = -0.3$ and $\mathrm{Pr} = 7$.

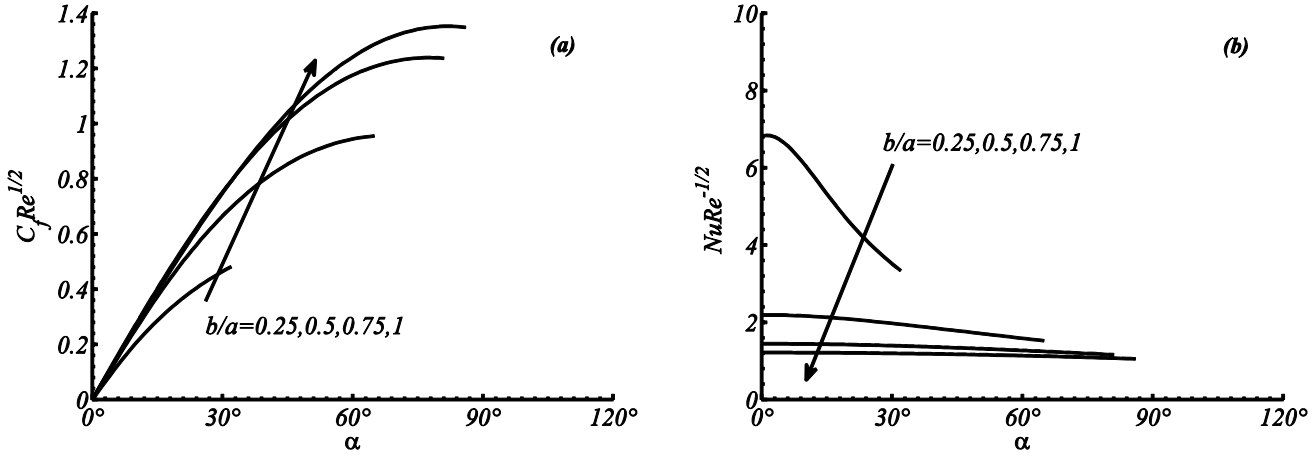

Figs. 9(*a*,*b*): The variation of $C_f \,\mathrm{Re}^{\frac{1}{2}}$ and $Nu\,\mathrm{Re}^{-\frac{1}{2}}$ for the various values of parameter $\frac{b}{a}$ with $K = 0.2$, $\lambda = 2$ and $\mathrm{Pr} = 7$.

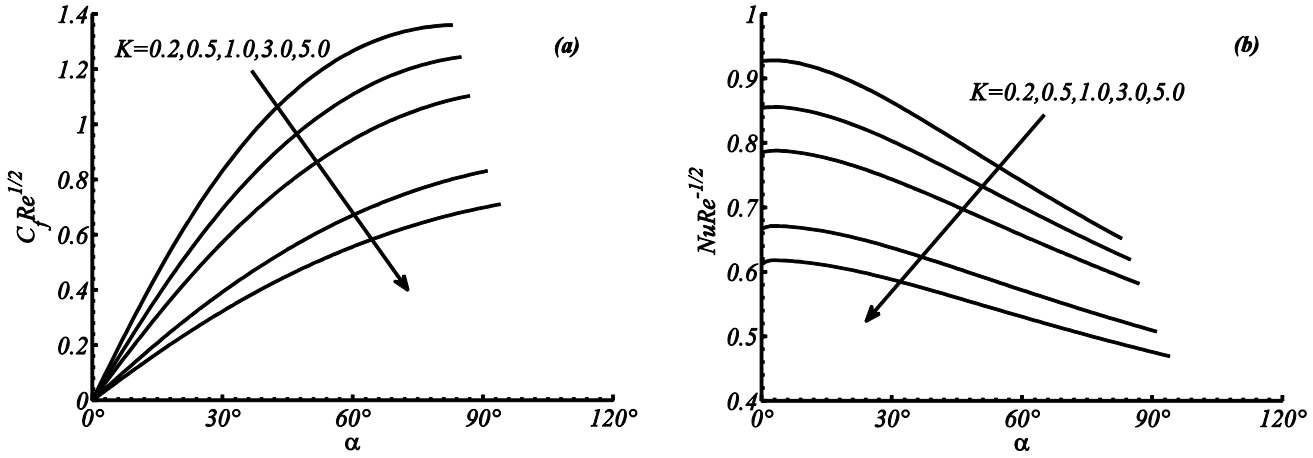

Figs.10(*a,b*): The variation of $C_f \, \mathrm{Re}^{\frac{1}{2}}$ and $Nu \, \mathrm{Re}^{-\frac{1}{2}}$ for various values of viscoelastic parameter K when $\lambda = 1$, $b/a = 0.5$ and $\mathrm{Pr} = 1$.

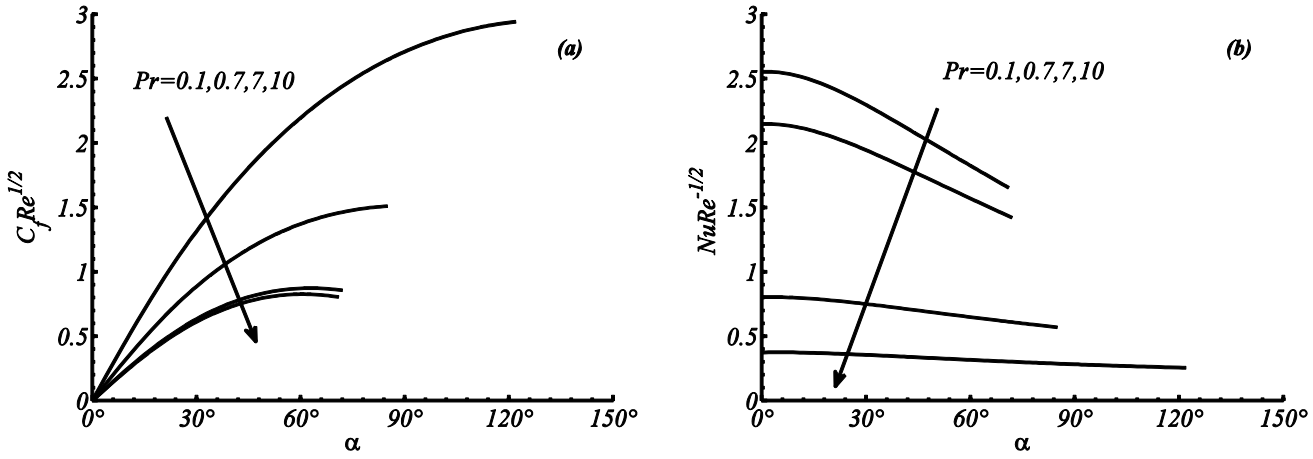

Figs. 11(*a,b*): The change in $C_f \, \mathrm{Re}^{\frac{1}{2}}$ and $Nu \, \mathrm{Re}^{-\frac{1}{2}}$ for various values of Prandtl number Pr when $\lambda = 1$, $b/a = 0.5$ and $K = 0.2$.

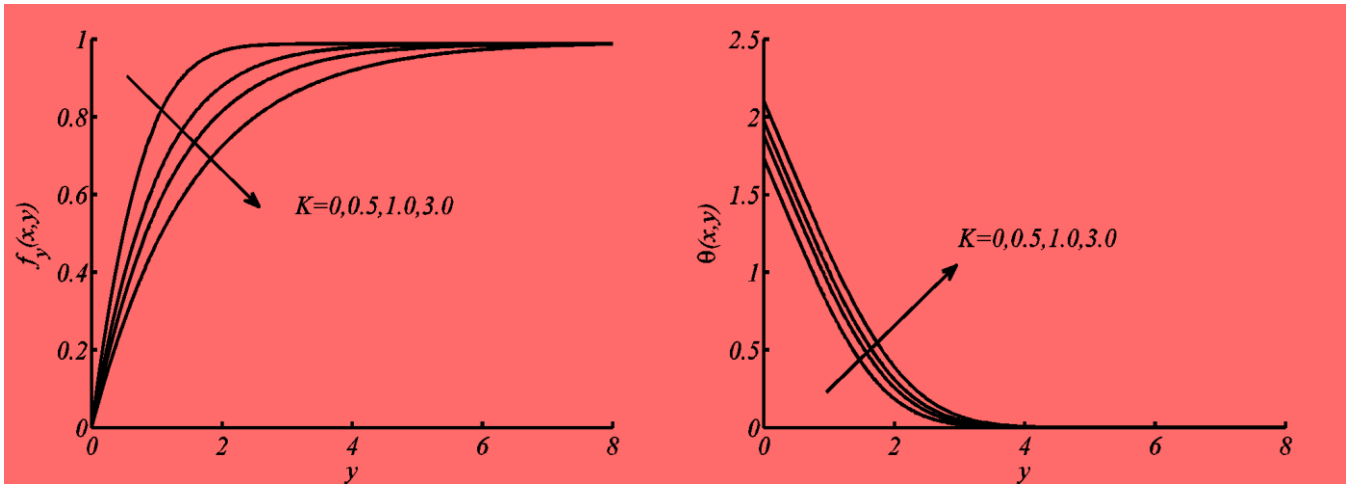

Figs. 12(*a,b*): The variation in velocity and temperature in case of blunt orientation for various values of viscoelastic parameter K when $\lambda = 2$, $b/a = 0.5$ and $\mathrm{Pr} = 1$.

Figs. 10 (a,b) display the trends of both flow and heat transfer rates for various values of the Prandtle number Pr. It is noticed that both quantities decline with the rise in value of Prandtle number Pr. Figs.11 (a,b) show the velocity and temperature profile in the boundary layer for various options of viscoelastic parameter K at the

eccentric angle $\alpha = 30^0$ in the blunt orientation case. The velocity reduces due to the increase in viscoelasticity of the fluid on the other hand temperature increases in the boundary layer.

5. Conclusion

In the present theoretical study, we investigated the mixed convection boundary layer flow of a viscoelastic fluid over the surface of a horizontal cylinder of elliptic cross section subjected to a constant surface heat flux. The boundary layer equations governing the flow and heat transfer are transformed to non-dimensional, nonlinear system of P.D.E's which is solved by an efficient finite difference scheme (Keller-box method). The effects of viscoelasticity, mixed convection parameter, aspect ratio parameter and the Prandtl number over the flow and heat transfer rates are carefully observed. The present study provides a useful data for devising a most efficient cooling system. It leads to the following inferences:

- By increasing the value of mixed convection parameter, both flow and heat transfer rates enhanced for both the orientations.
- In cooled cylinder case, flow and heat transfer rates reduces in blunt orientation by increasing the aspect ratio but in slender orientation both flow and heat transfer rates increase for $0 < b/a < 0.5$ and decrease for $0.5 < b/a < 1$.
- In heated cylinder case, the flow rate increases in both blunt and cylinder orientations with increase in the aspect ratio whereas heat transfer rate increases in slender orientation by the rise in aspect ratio. On the other hand, in blunt orientation it increases along the surface of cylinder in range $0 < \alpha < 42^\circ$ changes its behavior in $42^\circ < \alpha < 69^\circ$ and then decreases in $69^\circ < \alpha < 86^\circ$.
- Both flow and heat transfer rates decrease in the both orientation cases by enhancing the viscoelasticity of the fluid.
- The rise in Prandtl number results in reduction of both the flow and heat transfer rates in the blunt orientations and exhibit opposite behavior in the slender orientation.
- The velocity of the fluid in the boundary layer decreases but temperature rises by enhancing viscoelasticity of the fluid.

Nomenclature

a,b	Length of semi major and minor axes [m]
C_f	Skin friction coefficient [-]
C_p	Specific heat constant [$m^2s^{-2}K^{-1}$]
f	Dimensionless stream function [-]
g	Acceleration due to gravity [ms^{-2}]
Gr	Greshof number [-]
k	Thermal conductivity [$kgms^{-3}K^{-1}$]
k_0	Viscoelastic material parameter [kgm^{-1}]
K	Non-dimensional viscoelastic parameter [-]
Nu	Nusselt number [-]
Pr	Prandtl number [-]
q_w	Wall heat flux [kgs^{-3}]
Re	Reynolds number [-]
T	Temperature of the fluid in the boundary layer [K]
T_∞	Ambient fluid temperature [K]
T_w	Surface temperature [K]
U_∞	Free steam velocity [K]
$\bar{u},\bar{v}$	Velocity components in $\bar{x}$ and $\bar{y}$ directions, respectively [-]
$\bar{u}_e$	Free stream velocity
$\bar{x},\bar{y}$	Coordinates along and normal to the surface of cylinder respectively [m]
x, y	Cartesian coordinates along the surface and normal to the surface

Greek symbols

α	Eccentric angle [-]
β	Thermal expansion coefficient [K^{-1}]
θ	Dimensionless temperature [-]
θ_w	Surface temperature parameter [-]
ρ	Fluid density [kgm^3]
μ	Dynamic viscosity
ν	Kinemic viscosity [m^2s^{-1}]
λ	Mixed convection parameter [-]
τ_w	Surface shear stress [$kgm^{-1}s^{-2}$]
ψ	Dimensionless stream function [-]

Subscripts

Superscript

w	Condition at the surface	$'$	Differentiation with respect to y
∞	Condition far away from the surface		

References

[1] Merkin, J.H., Free convection boundary layers on cylinders of elliptic cross section, *J. Heat Transfer 99* (1977), pp. 453-457.

[2] Merkin, J.H., Mixed convection from a horizontal circular cylinder, *Int. J. Heat Mass Transfer 20* (1977), pp. 73-77.

[3] Bhatacharyya, S. and Pop, I., Free convection from cylinder of elliptic cross section in micropolar fluids, *Int. J. Eng. Sci. 34* (1996), pp.1301-1310.

[4] M.A. Hossain, M.A. Alim, D. Rees, Effect of thermal radiation on natural convection over cylinders of elliptic cross section, *Acta Mech. 42* (1998), pp. 177-186.

[5] S. Ahmad, N.M. Arifin, R. Nazar and I. Pop, Free convection boundary layer flow over cylinders of elliptic cross section with constant surface heat flux, *Eur. J. Sci. Res. 23* (2008), pp. 613-625.

[6] T. Javed, I. Mustafa, H. Ahmad, Effect of thermal radiation on unsteady mixed convection flow near forward stagnation point over a cylinder of elliptic cross section, *Thermal science,* doi: 10.2298/tsci140926027j (2015).

[7] T. Javed, H. Ahmad, A. Ghaffari, Mixed convection boundary layer flow over a horizontal elliptic cylinder with constant heat flux, *Z. Angew. Math. Phys., 66* (2015), 6, pp. 3393-3403.

[8] Rashidi, M. M., et al. Mixed convective heat transfer for MHD viscoelastic fluid flow over a porous wedge with thermal radiation, *Advances in Mechanical Engineering 6* (2014), pp. 735939.

[9] Garoosi F., et al., Two-phase mixture modeling of mixed convection of nanofluids in a square cavity with internal and external heating, *Powder Technology 275* (2015), pp. 304-321

[10] Bég, O. A, et al. Double-diffusive radiative magnetic mixed convective slip flow with Biot and Richardson number effects, *Journal of Engineering Thermophysics, 23* (2014), 2, pp. 79-97.

[11] Rashidi, M. M., et al. Group theory and differential transform analysis of mixed convective heat and mass transfer from a horizontal surface with chemical reaction effects, *Chemical Engineering Communications, 199* (2012), 8, pp. 1012-1043.

[12] J.E. Dunn, K.R. Rajagopal, Fluids of differential type: critical review and thermodynamic analysis, *Int. J. Eng. Sci. 33* (1995), pp. 689-729.

[13] P.D. Ariel, Stagnation point flow of a viscoelastic fluid towards a moving plate, *Int. J. Eng. Sci. 33* (1995), pp. 1679-1687.

[14] K.R. Rajagopal, M. Renardy, Y. Renardy, A.S. Wineman, Flow of viscoelastic fluids between plates rotating about distinct axes, *Rheol.Acta 25* (1986), pp. 459-467.

[15] R.A. Cortell, Note on flow and heat transfer of a viscoelastic fluid over a stretching sheet, *Int. J. Non-Linear Mech. 41* (2006), pp. 78-85.

[16] M.S. Abel, S.K. Khan, K.V. Prasad, Study of visco-elastic fluid flow and heat transfer over a stretching sheet with variable viscosity, *Int. J. Non-Linear Mech. 37* (2002), pp. 81-88.

[17] T. Hayat, Z. Abbas, T. Javed, Mixed convection flow of a micropolar fluid over a nonlinear stretching sheet, *Physics Letters A372* (2008), pp. 637-647.

[18] M. Sajid, Z. Abbas, T. Javed, N. Ali, Boundary layer flow of an Oldroyed B fluid in the Region of stagnation point over a stretching sheet, *Canadian J. of Physics, 88* (2010), pp. 635-640.

[19] Abbas, Z., et al., Mass transfer in two MHD viscoelastic fluids over a shrinking sheet in porous medium with chemical reaction species, *J. Porous Media 16* (2013), 7, pp. 619-636

[20] Abbas, Z., et al., Hydromagnetic stagnation point flow of a micropolar viscoelastic fluid towards a stretching/shrinking sheet in the presence of heat generation, *Can. J. Phys. 92* (2014), 10, pp. 1113-1123

[21] Abbas, Z., et al., Chemically reactive hydromagnetic flow of a second grade fluid in a semi-porous channel, *J. Appl. Mech. Tech. Phys. 56* (2015), 5, pp. 878-888

[22] Anwar, I. et al., Mixed convection boundary layer flow of a viscoelastic fluid over a horizontal circular cylinder, *Int. J. Non-Linear Mech. 43* (2008), pp. 814-821.

[23] Kasim, A.R.M et al., Constant heat flux solution for mixed convection boundary layer viscoelastic fluid, *Heat Mass Transfer, 49*(2013), pp. 163–171.
[24] Ahmad, H., Javed, T., Ghaffari, A., Radiation effect on mixed convection boundary layer flow of a viscoelastic fluid over a horizontal circular cylinder with constant heat flux, *Journal of Applied Fluid Mechanics*, *9*(2016), 3, pp. 1167-1174.
[25] Garg, V.K. and Rajagopal, K.R., Stagnation point flow of a non-Newtonian fluid, *Mech. Res. Commun. 17* (1990), pp. 415-421.
[26] Keller, H.B. and Cebeci, T., Numerical methods in boundary layer theory, *Annual Rev. Fluid Mech. Vol. 10* (1978), pp. 417-33.
[27] Cebeci, T. and Bradshaw, P., *Physical and Computational Aspects of Convective Heat Transfer,* Springer New York (1984).
[28] Nazar, R. et al., Mixed convection boundary layer flow from a horizontal circular cylinder with a constant surface heat flux, *Int. J. Heat Mass Transfer 40*(2004), pp. 219-227.